Plasma Conditions Generated by Interaction of a High Brightness, Prepulse Free, Raman Amplified KrF Laser Pulse with Solid Targets

D. Riley, L. A. Gizzi, F. Y. Khattak, A. J. Mackinnon, S. M. Viana, and O. Willi
The Blackett Laboratory, Imperial College of Science, Technology and Medicine, Prince Consort Road, London SW7 2BZ, United Kingdom
(Received 10 April 1992)

A high brightness, Raman amplified KrF laser has been used to irradiate solid targets with 12 ps laser pulses at intensities above 10^{15} W/cm^2 without the presence of a preformed plasma caused by low level amplified spontaneous emission prepulse. Time-resolved x-ray spectroscopy of the *K*-shell emission from aluminum was used to infer electron densities in excess of 10^{23} cm^{-3} at temperatures of several hundred electronvolts.

PACS numbers: 52.50.Jm

Interest in the production of dense, hot plasmas by irradiation of solids with short pulse lasers is largely motivated by applications to x-ray laser research where rapid heating at high density is required. Several workers have published experiments in which, mostly time-integrated, spectroscopy is used to diagnose plasmas created by irradiation of solid targets with laser pulses of subpicosecond to a few tens of picoseconds duration [1–6].

We have carried out an experiment in which an effectively prepulse free, high brightness (3× diffraction limited divergence), Raman amplified KrF pulse [7] interacted with solid targets. The laser pulses were of 12 ps full width at half maximum (FWHM) duration and Raman shifted in methane to 268 nm wavelength. The amplified spontaneous emission (ASE) prepulse to main pulse power (energy) ratio was below the 10^{-10} (10^{-8}) detection threshold, implying no preformed plasma production for irradiances up to the 10^{17} W/cm^2 used. About 4 J of laser energy was directed onto planar, 25 μm thick, aluminum foils by an off-axis paraboloid, with $f/4$ focusing.

A time-resolving x-ray spectrometer, consisting of a thallium-hydrogen-phthalate crystal ($2d = 2.58$ nm) coupled to an x-ray streak camera which was fitted with a KBr photocathode, was used to record the Al *K*-shell emission from 6 to 7 Å with temporal and spectral resolutions of 10 ps and 350, respectively, viewing the plasma at 35 deg to the target normal. The focal spot was monitored via an x-ray pinhole camera with ×15 magnification. The 10 μm diam pinhole was filtered to be sensitive to the bremsstrahlung and radiative recombination x rays (around 2.5 keV) which are primarily generated during the laser pulse. Approximately 90% of the x-ray emission was contained within the FWHM intensity. The absorbed energy was obtained by measuring the scattered light with an Ulbricht sphere and a diode on a backscatter channel, both of which were calibrated *in situ*. The absorbed fraction ranged from around 60% down to 10% for irradiances from 10^{14} W cm^{-2} up to 10^{17} W cm^{-2}. A more detailed description of the absorption and interaction of the beam with solid targets, including ion cup and x-ray *p-i-n* diode data, will be presented at a later date.

Figure 1(a) shows streak data for an aluminum target irradiated at approximately 6×10^{15} W cm^{-2}. Note the temporal evolution of the higher He-like line series from a broad emission band into distinct lines, indicating high electron density at the start of the emission. This is seen

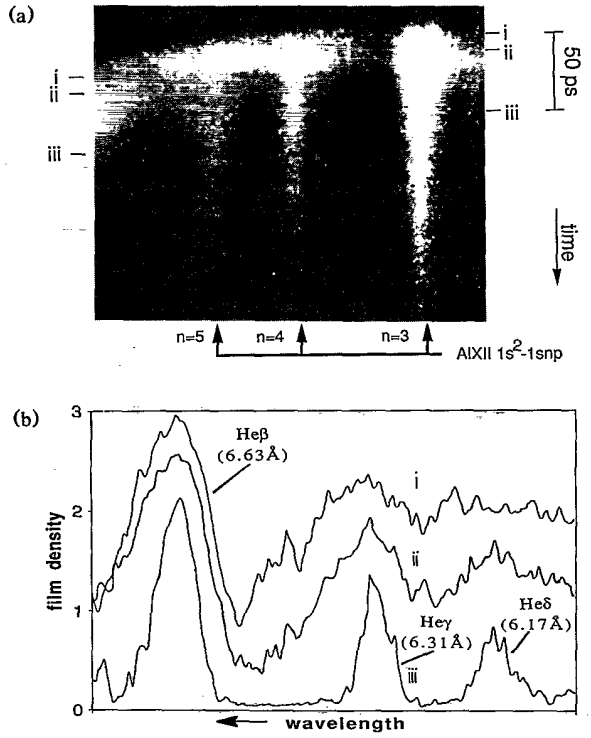

FIG. 1. (a) Streaked x-ray spectrum of He-like line series. (b) Film density lineouts showing He-like transitions and the line-center wavelengths. Timing is (i) 10 ps before peak Ly-β emission, (ii) at the peak, and (iii) 40 ps after the peak. Scan (i) is displaced up in density by 0.3. The image curvature, due to electron path differences in the camera, introduces a timing difference across the scans of the order of the temporal resolution.

clearly in the film density lineouts of Fig. 1(b), which shows an emission band, well above the bremsstrahlung continuum at early time [scan (i)], which evolves into distinct AlXII $1s^2$-$1s4p$ (He_γ) and $1s^2$-$1s5p$ (He_δ) transitions in scans (ii) and (iii). Figure 2 shows time-integrated data taken for similar conditions by placing x-ray film in front of the cathode. The main feature is the narrower, well-defined lines which contrast with scans (i) and (ii) of Fig. 1(b) and are qualitatively more comparable to scan (iii). A reason for the difference between time-integrated and time-resolved data is discussed below.

In order to assess the plasma conditions more closely, we analyzed similar data taken with lower dispersion. This meant that the spectra included the AlXIII $1s$-$3p$ (Ly-β) transition, and the temperature is indicated by the ratio of He-like to H-like emission. The evolution of the He_γ and He_δ lines from a broad band into distinct transitions was also seen for these data shots. The electron density was determined from the Stark width of the He_β (AlXII $1s^2$-$1s3p$) and Ly-β transitions. The variation of linewidth with density was calculated with the spectral simulation code SPECTRA [8] which includes detailed Stark profiles, continuum lowering, opacity, Doppler broadening, and instrument width. The temperature was assumed to be 400 eV for He_β and 600 eV for Ly-β, but to account for uncertainty in opacity, was varied from 200 to 800 eV and 300 to 900 eV for He_β and Ly-β, respectively. The mean plasma ρR was varied up to 1.2×10^{-4} g cm^{-2}. These conditions were chosen to span the expected values for the emission region. The variation in predicted density for a given linewidth is used to set the error bars for experimentally inferred density. A fit of the full line profile was carried out on a few scans; the results obtained were the same as for the FWHM comparison to well within the error bars. Instrument broadening made the linewidth insensitive to density below about 3×10^{22} cm^{-3}. For electron densities of around 10^{23} cm^{-3}, the SPECTRA code predicts a spectrum similar to scan (i) of Fig. 1(b).

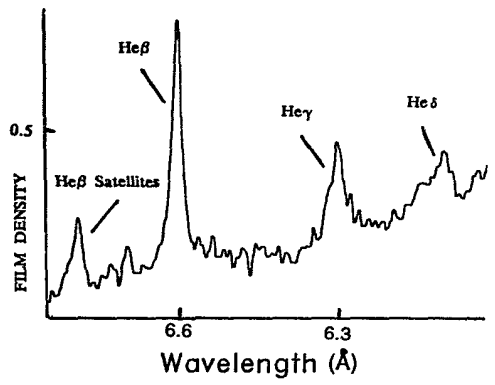

FIG. 2. Time-integrated spectrum for $I=5\times10^{15}$ W cm^{-2}. The Ly-β line was cut off by the film pack. The width of the He_γ line suggests the electron density is about 1×10^{22} cm^{-3}.

The experiment was simulated with a 1D hydrocode, MEDUSA [9], in which the heat flow is given by the smaller of the Spitzer value and a flux limited free streaming limit. From the work of Rickard, Bell, and Epperlein [10], we chose a flux limit of 0.1. The energy is absorbed by inverse bremsstrahlung and resonance absorption. The resonance absorption fraction is set at each time step by calculating the scale length [11] at critical density and averaging the angle of incidence for $f/4$ focusing. Some resonantly absorbed energy is dumped at critical density. The rest is put into hot electrons which are transported in ten energy groups with an initial temperature at critical density, given by the expression derived from experiments by Giovanielli [12]. The fraction of resonantly absorbed energy assigned to hot electrons did not significantly alter the hydrodynamic behavior, because the relatively low suprathermal electron temperature (4.5 keV for $I=4.0\times10^{15}$ W cm^{-2}) meant that the hot electron energy was dumped spatially close to the critical density surface anyway. For the simulations presented here, around 5% of the incident energy went into hot electrons. The ionization balance is calculated with a time-dependent non-local-thermodynamic-equilibrium average atom (AA) model similar to XSN [13]. Because the AA model treats ions in a hydrogenic approximation it might be expected to give reasonable results as the plasma is dominated by the He-like to bare ions. The AA model has been compared with a detailed ionization model [8,14] in the steady-state case. For electron temperatures and densities between 200 and 900 eV and 10^{22} and 10^{23} cm^{-3}, respectively, the two models gave the ratio of bare to hydrogenic ions to within at most a factor of 2 with differences less than 20% for most of the conditions of interest. The emission of the AlXII $1s^2$-$1s3p$ and AlXIII $1s$-$3p$ lines was calculated by assuming that their upper levels were in local thermodynamic equilibrium (LTE) with the bare and hydrogenic ground states, respectively. This should be a reasonable assumption at above critical electron density of 1.55×10^{22} cm^{-3} [15]. The effect of hot electrons on the ionization balance is not included in our modeling; however, the simulations suggest that few hot electrons reach the high density plasma emitting at early time and they are not expected to significantly alter our conclusions about the plasma conditions.

The expected line profile was calculated by summing the predicted profiles (including Doppler shifting) for each cell, which were normalized according to the number of emitting ions. Because we do not yet have a full radiative transfer model with proper Stark profiles to account for the changing line shape and Doppler shift through the plasma, we have approximated the effective optical depth for emission from each cell by summing ground-state ion densities in the other cells through which the emission is viewed experimentally. Simulations carried out in an optically thin approximation yield a 7% narrower FWHM linewidth at the peak electron density.

This indicates that our approximation will not result in large errors.

In Fig. 3 we compare predicted and measured FWHM linewidths on the left-hand coordinate axis. On the right-hand coordinate axis, we interpret the experimental linewidth in terms of an electron density for an average plasma ρR and T_e, as discussed above. The vertical error bars refer only to the density scale and are reasonably large simply because of the wide range of plasma conditions used in converting linewidth to density. This makes our conclusions about the electron density as independent as possible of the detailed conditions predicted by the hydrocode. In order to make the comparison, the times of peak Ly-β emission for simulation and experiment were equated. In both simulation and experiment the peaks of the He$_\beta$ and Ly-β were separated by less than the 10 ps resolution (image curvature was accounted for). The predicted laser energy absorption of 41% was consistent, to within a few percent, with measurements. The peak linewidth and general falloff are reasonably well reproduced by the hydrocode. Weak emission at early time precludes the observation of the initial density rise.

Referring to Fig. 1(b), the width of the He$_\beta$ line in scan (i) indicates an electron density of approximately 1.4×10^{23} cm^{-3}. With the continuum lowering model of Stewart and Pyatt [16], for temperatures when He-like emission is strong (few hundred electronvolts), we expect the He-like $1s^2$-$1s5p$ transition to be present in the spectrum. For an almost fully ionized plasma, the merging of the He$_\gamma$ and He$_\delta$ lines is consistent with the Inglis-Teller model [17] of line series merging at high electron density. We note that, because emission from lower densities is weighted towards the line center, the average density of emission predicted by simulation at the pulse peak for the data in Fig. 3 is about 25% higher than given by the predicted linewidth.

Figure 4(a) shows the predicted He$_\beta$/Ly-β line ratio, compared to experiment for times when the electron density of the emitting region allows the LTE approximation. At the average irradiance, the predicted ratio is generally within a factor of 2 of the measured value. The predicted typical temperature, shown in Fig. 4(b), is defined by finding the emission weighted average temperatures for the He-like and H-like lines separately and taking their mean. As can be seen, the variation in temperature that would bring the predicted and measured line ratios into agreement is generally less than 100 eV. The maximum difference in the emission temperatures for He-like and H-like lines occurs at around peak emission ($t=20$ ps in

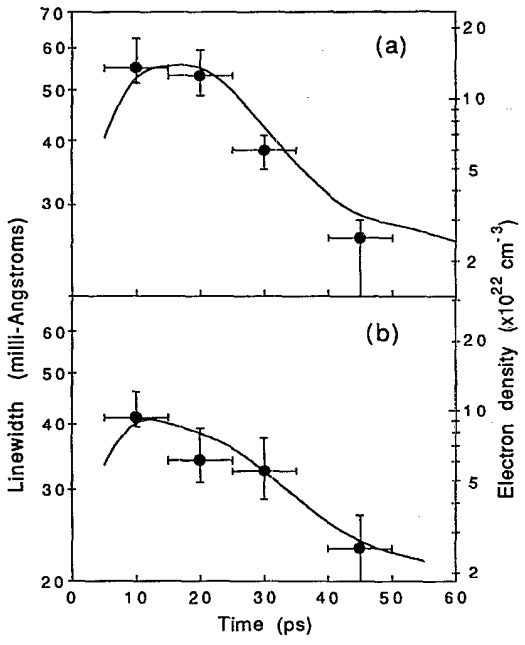

FIG. 3. Time history of predicted linewidth (solid line) vs measured linewidth (solid circles) for (a) He$_\beta$ and (b) Ly-β lines. A 10 ps window is folded into the predicted data to simulate temporal resolution. The error bars only refer to the right-hand coordinate axis where the measured linewidth is converted to electron density. They result from varying assumed conditions around the average as described in the text.

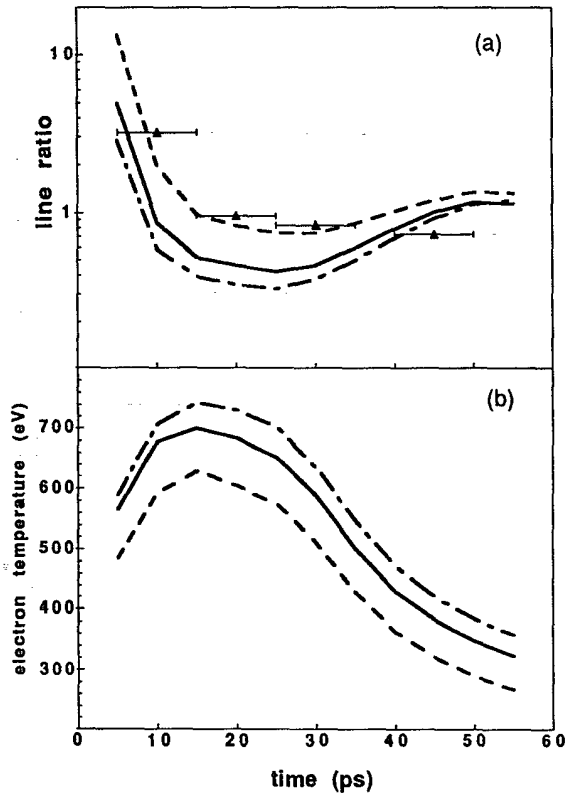

FIG. 4. (a) Measured He$_\beta$/Ly-β line ratio vs simulation for irradiances of 2×10^{15} W cm^{-2} (dashed line), 4×10^{15} W cm^{-2} (solid line), and 6×10^{15} W cm^{-2} (dot-dashed line). (b) Predicted average plasma emission temperature for the same irradiances, with same line styles as (a). Again a 10 ps window is folded into predicted data.

the simulation). For $I=4\times10^{15}$ W cm^{-2}, these are 620 and 780 eV, respectively. The similarity of predicted temperature and measured electron density for the He-like and H-like lines suggests that the plasma is both hot and dense at the same time.

The simulated FWHM duration of emission is 20 and 25 ps for the He$_\beta$ and Ly-β lines, respectively, which compares well with the measured value of 25–30 ps for both lines. However, the streak data in Fig. 1(a) show a strong tail of emission lasting about 100 ps. By using a low-density CsI cathode which is much more sensitive to low level signals, but with poor temporal resolution (about 50 ps), we observed Ly-β emission lasting longer than 1 ns, mostly with a linewidth comparable to the instrument width. The simulations above, using LTE in excited states, suggest as an upper limit that over 90% of the He$_\beta$ and 70% of Ly-β emission comes after 50 ps. This is without detailed modeling of the effect of line trapping on the ionization balance, but shows that it is possible that the major part of the time-integrated emission comes at late time and from low density plasma. We believe that the long tail of emission accounts for the difference in linewidth between our time-integrated and time-resolved data and that a similar effect probably causes the narrow linewidths seen in time-integrated data where the targets are transparent to the ASE [6].

In conclusion, we have demonstrated the production of a rapidly heated, dense plasma with a high brightness, prepulse free, Raman amplified KrF laser. In particular, the observation of line series merging for the He-like aluminum lines, supports the measurement of high electron density from the Stark linewidths. The use of time resolution has resulted in spectral features that differ markedly from those obtained with time-integrated spectroscopy in the same experiment.

The authors would like to thank the staff of the Central Laser Facility at the Rutherford Appleton Laboratory who made this work possible. We also thank Dr. J. Edwards for helpful discussions and Dr. R. W. Lee for supplying the SPECTRA code. This work was funded by the SERC.

[1] C. H. Nam, W. Tighe, S. Suckewer, J. F. Seely, U. Feldman, and L. A. Woltz, Phys. Rev. Lett. **59**, 2427 (1987).
[2] J. A. Cobble, G. A. Kyrala, A. A. Hauer, A. J. Taylor, C. C. Gomez, N. D. Delameter, and G. T. Schappert, Phys. Rev. A **39**, 454 (1989).
[3] M. M. Murnane, H. C. Kapteyn, and R. W. Falcone, Phys. Rev. Lett. **62**, 155 (1989).
[4] G. J. Tallents, M. H. Key, P. Norreys, D. Brown, J. Dunne, and H. Baldis, Phys. Rev. A **40**, 2857 (1989).
[5] O. Willi, G. Kiehn, J. Edwards, V. Barrow, R. A. Smith, J. Wark, and E. Turcu, Europhys. Lett. **10**, 141 (1989).
[6] A. Zigler, P. G. Burkhalter, D. J. Nagel, M. D. Rosen, K. Boyer, T. S. Luk, A. McPherson, and C. K. Rhodes, Opt. Lett. **16**, 1261 (1991).
[7] I. N. Ross, M. J. Shaw, C. J. Hooker, M. H. Key, E. C. Harvey, J. M. D. Lister, J. E. Andrew, G. J. Hirst, and P. A. Rodgers, Opt. Commun. **78**, 263 (1990); E. C. Harvey, C. J. Hooker, J. R. Houliston, M. H. Key, A. K. Kidd. J. M. D. Lister, I. N. Ross, and M. J. Shaw, Rutherford-Appleton Laboratory Report No. RAL-91-025 (1991), p. 77.
[8] R. W. Lee, B. L. Whitten, and R. E. Stout, II, J. Quant. Spectrosc. Radiat. Transfer **32**, 91 (1984).
[9] J. P. Christiansen, D. E. T. F. Ashby, and K. V. Roberts, Comput. Phys. Commun. **7**, 271 (1974).
[10] G. J. Rickard, A. R. Bell, and E. M. Epperlein, Phys. Rev. Lett. **62**, 2687 (1989).
[11] T. P. Hughes, in *Proceedings of the Twentieth Scottish Summer School in Physics*, edited by R. A. Cairns and J. J. Sanderson (SUSSP Publications, University of Edinburgh, Edinburgh, 1979).
[12] D. N. Giovanielli, Bull. Am. Phys. Soc. Ser. II **9**, 1047 (1976).
[13] W. A. Lokke and W. H. Grasberger, Lawrence Livermore National Laboratory Report No. UCRL-52276, 1977 (unpublished); P. A. Rodgers, A. M. Rogoyski, and S. J. Rose, Rutherford-Appleton Laboratory Report No. RAL-89-127, 1989 (unpublished).
[14] V. A. Barrow, Ph.D. thesis, University of London, 1991 (unpublished).
[15] H. R. Griem, *Plasma Spectroscopy* (McGraw-Hill, New York, 1964).
[16] J. Stewart and K. Pyatt, Astrophys. J. **144**, 1203 (1966).
[17] D. R. Inglis and E. Teller, Astrophys. J. **90**, 439 (1939).